RSC Advances

ROYAL SOCIETY OF CHEMISTRY

www.rsc.org/advances

Submit to RSC Advances (RA-ART-09-2014-010978 R1)

Nickel sulfide film with significantly enhanced electrochemical performance induced by self-assembly of 4-aminothiophenol and their application in dye-sensitized solar cells

Gentian Yue [a *], Fumin Li [a], Furui Tan [a], Guoqiang Li [a], Chong Chen [a], Jihuai Wu [b]

[a] *Key Laboratory of Photovoltaic Materials of Henan and School of Physics & Electronics, Henan University, Kaifeng 475004, China*;

[b] *Institute of Material Physical Chemistry, Huaqiao University, Quanzhou 362021*;

Keywords: Nickel sulfide; self-assembly; counter electrode; dye-sensitized solar cell; photoelectric properties

∗ Corresponding author. Tel.: +86 371 23881602, E-mail address: yuegentian@126.com (G. Yue).

Abstract: Dye-sensitized solar cell (DSSC) is a promising solution to global energy and environmental problems because of its clean, low-cost, high efficiency, good durability, and easy fabrication. However, seeking platinum (Pt)-free CE alternative with high electrocatalytic activity and low cost to enhance the efficiency of the DSSC still is a key issue. In this study, a novel composite film of 4-aminothiophenol/nickel sulfide (4-ATP/NiS) was prepared by two-step chemical/electrochemical process and served as CE for DSSC. The surface morphology of the 4-ATP/NiS composite film was characterized by field emission scanning electron microscopy (FESEM) and showed a microporous structure. The electrochemical performance of the 4-ATP/NiS (here marked as NiS*) counter electrode (CE) was evaluated by cyclic voltammetry (CV), electrochemical impedance spectroscopy (EIS) and Tafel curves, which revealed that the NiS* CE possessed excellent electrocatalytic activity for the reduction reaction of triiodide to iodide and low charge transfer resistance at the interface between electrolyte and CE, respectively. The DSSC assembled with the novel NiS* CE achieved an enhanced power conversion efficiency of 7.20% under the irradiation of 100 $mW \cdot cm^{-2}$ as comparing to that of the DSSC based on Pt electrode. Thus, this concept and therefore significant enhancement in power conversion efficiency can be applied other DSSCs with Pt-free CEs such as polyaniline, poly (3, 4-ethylenedioxythiophene), graphene and so on.

1. Introduction

Substantial efforts have been devoted to improve the power conversion efficiency (*PCE*) of the dye-sensitized solar cell (DSSC) since its first prototype was reported in 1991.[1] The highest *PCE* of DSSC has achieved over 12%.[2] Nowadays, how to enhance the efficiency and reduce costs of the DSSC are the major challenges. As an important component of DSSC, CE plays a crucial role in the performance of DSSC. An ideal CE should be of excellent electrocatalytic activity and high conductivity for the redox reaction, low-cost, small overpotential and long-term stability in the electrolyte.

Currently, the most widely used CE in DSSC is Pt electrode, which is prepared by thermal decomposition,[3] electrodeposition,[4] chemical reduction[5] or sputtering.[6] However, Pt as the expensive noble metal impeded the commercialization of DSSCs.[7] In order to resolve the issues, various types of Pt-free CEs alternative have been studied, e.g., carbon materials,[8-10] conducting polymers,[11,12] transition metal sulfides,[13-15] nitrides[16] and as well as carbides.[17] Among them, nickel sulfide (NiS) as a promising candidate meets developmental and environmental goals, along with an ideal CE material requirement. The DSSC based on a NiS CE electrodeposited by a potential reversal technique showed a comparable performance (6.82%) to the Pt-based (7.00%).[18] Highly transparent NiS CE was prepared by an electrodeposition technique and presented a good photovoltaic performance for thiolate/disulfide mediated DSSCs.[19] Therefore, NiS is a good candidate for an efficient CE.

Traditionally, the transparent conductive oxide (TCO) supported NiS CE was prepared by electrodeposition or hydrothermal method. However, there are few reports on in situ synthesis of NiS on TCO modified by 4-aminothiophenol (4-ATP) ethanol solution as a CE for DSSCs so far. Herein, we prepared a novel composite film of 4-ATP/NiS (marked as NiS*) as CE for DSSC by two-step chemical/electrochemical process. To accelerate the charge transfer from FTO to NiS, 4-ATP was used as a bridging agent via a covalent bonding between FTO and -SH end on 4-ATP and NiS end on 4-ATP, showing a great improvement electrochemical behavior to iodide/triiodide. According to the characterization by FE-SEM, CV, EIS and Tafel polarization exhibited a flat surface with a microporous structure, excellent electrocatalytic activity and low charge transfer

resistance on electrolyte/electrode interface. The DSSC with NiS* CE achieved an enhanced photovoltaic conversion efficiency of 7.20% under the irradiation of 100 $mW \cdot cm^{-2}$ (AM 1.5G simulated solar light).

2. Experimental

2.1 Materials

The nickel (II) chloride hexahydrate ($NiCl_2 \cdot 6H_2O$, 98%), thiourea (TU, ≥ 99.0%), ethanol (≥ 99.5%), 4-tert-butyl-pyridine (TBP), 4-aminothiophenol (4-ATP) (purity 98%) and titanium tetrachloride ($TiCl_4$) were purchased from Shanghai Chemical Agent Ltd., China. All reagents are of analytical reagent grade.

The organometallic compound sensitized dye Z-907 *cis*-bis (isothiocyanato) (2, 2'-bipyridyl-4,4'-dicarboxylato) (2,2'-bipyridyl-4,4'-di-nonyl) ruthenium (II) is obtained from Solaronix SA (Switzerland). The FTO glass substrates (8 $\Omega \cdot cm^{-2}$, the thickness of 350 nm, Hartford Glass Co., USA) were cut into pieces with size of 1×2 cm^2 carefully and ultrasonically cleaned sequentially in detergent, acetone and distilled water for 30 min, respectively, which later stored in isopropyl alcohol.

2.2 Preparation of 4-ATP/NiS counter electrode

Modification of FTO glass by 4-ATP. FTO substrate was decorated with a self-assembly technique to form a uniform 4-ATP monolayer. The details described as following: the cleaned FTO glass was immersed in 4-ATP/ethanol solution ([4-ATP] 0.03 M) for more than 1 h, after being rinsed with deionized water and used for NiS deposition.

Briefly, the 4-ATP/NiS CE was prepared by using the electrochemical method which outlined below. The electrodeposition was carried out with an electrochemical analyzer system (CHI660B, Shanghai Chenhua Device Company, China). All experiments were implemented in a three-electrode cell, including one Pt foil as CE, one Ag/AgCl electrode as reference electrode, and 4-ATP/FTO substrate with an exposed area of 0.64 cm^2 as working electrode. TU was selected as the reducing agent and sulfur source. The base electrodeposition solution consisted of

$NiCl_2$ (0.05 M) and TU (1.0 M) in 50 ml deionized water and treated by ultrasonication for 30 min. A constant current density of 10 $mA \cdot cm^{-2}$ was served (the synthesis route shown in Scheme 1). The 4-ATP/NiS CE was put into anhydrous ethanol for 10 min and vacuum oven at 100℃ for 12 h, respectively. Then, the 4-ATP/NiS (NiS*) CE was obtained.

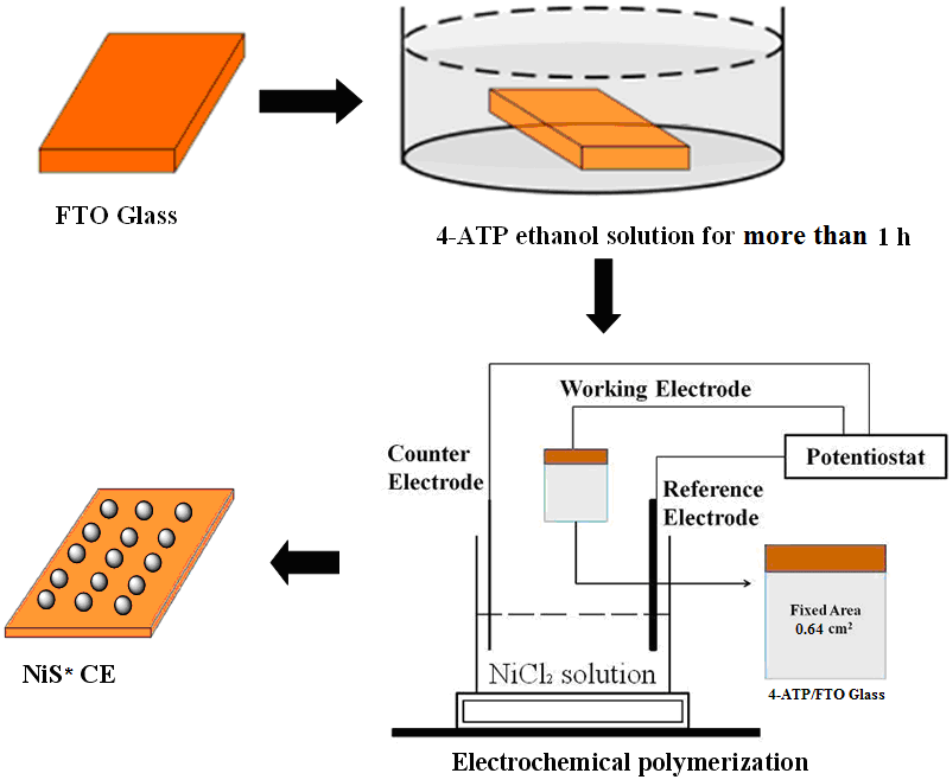

Scheme 1 Two-step chemical/electrochemical process of NiS* bilayer coated on FTO substrate.

2.3 Fabrication of DSSC

The TiO_2 anode was prepared as described previously.[20,21] A thin TiO_2 blocking layer was spin-coated on FTO substrate at 1500 rpm for 30 s, followed by sintering at 450℃ for 30 min in air. Subsequently, the TiO_2 layer with particle size of 10-20 nm was coated onto the blocking layer by using doctor blade method, and then sintered at 450℃ for 30 min in air, after being immersed in 0.15 M $TiCl_4$ solution at 70℃ for 0.5 h and sintering at 450℃ for another 30 min to form a reflect layer. The dye was loaded by soaking the TiO_2 anode in 0.3 mM of dye Z-907 ethanol solution for 12 h. Thus the dye-sensitized TiO_2 anode with thickness of 8-10 μm was obtained.

The DSSC was fabricated by injecting the liquid electrolyte (0.05 M of I_2, 0.1 M of LiI, 0.6 M of tetrabutylammonium iodide and 0.5 M of TBP in acetonitrile) into the aperture between the dye-sensitized TiO_2 anode and the CE. The two electrodes were clipped together and wrapped with thermoplastic hot-melt Surlyn.

2.4 Characterization

The surface morphology of the sample was observed by using JSM-7001F FE-SEM. Energy dispersive spectroscopy analysis (EDS) was obtained from Bruker-ASX (Model Quan-Tax 200). CV, EIS and Tafel polarization curves were conducted by using a computer-controlled electrochemical analyzer (CHI 660B, CH Instrument). The electrolyte used in the DSSC test was also injected into the symmetric dummy cells for EIS and Tafel measurements. EIS was carried out under the simulating open-circuit conditions at ambient atmosphere, sealing with thermoplastic hot-melt Surlyn and leaving an exposed area of 0.64 cm^2. The frequency of applied sinusoidal AC voltage signal was varied from 0.1 Hz to 10^5 Hz and the corresponding amplitude was kept at 5 mV in all cases.

The photovoltaic test of DSSC with an exposed area of 0.28 cm^2 was carried out by measuring photocurrent-photovoltage (*J-V*) character curve under white light irradiation of 100 $mW \cdot cm^{-2}$ (AM 1.5 G) came from the solar simulator (XQ-500W, Shanghai Photoelectricity Device Company, China) in ambient atmosphere. The fill factor (*FF*) and the power conversion efficiency (*PCE*) of DSSC were calculated according to the following equations:

$$PCE(\%) = \frac{V_{max} \times J_{max}}{P_{in}} \times 100\% = \frac{V_{oc} \times J_{sc} \times FF}{P_{in}} \times 100\% \quad (1)$$

$$FF = \frac{V_{max} \times J_{max}}{V_{oc} \times J_{sc}} \quad (2)$$

where J_{sc} is the short-circuit current density ($mA \cdot cm^{-2}$); V_{oc} is the open-circuit voltage (V); P_{in} is the incident light power ($mW \cdot cm^{-2}$) and J_{max} ($mA \cdot cm^{-2}$) and V_{max} (V) are the current density and voltage at the point of maximum power output in the *J–V* curve, respectively.

The exchange current density (J^0) and the limiting diffusion current density (J_{lim}) for the Tafel curves can be estimated according to equation (3) and (4):

$$J_0 = \frac{RT}{nFR_{ct}} \quad (3)$$

$$D = \frac{l}{2nFC} J_{\lim} \quad (4)$$

where R is the gas constant; n (n=2) is the number of electrons involved in the reduction of triiodide at the electrode; D is the diffusion coefficient of the triiodide; l is the spacer thickness; T is the temperature; F is Faraday's constant; R_{ct} is the charge transfer resistance; C is the triiodide concentration.

3. Results and discussion

3.1 Catalytic mechanisms of NiS CE*

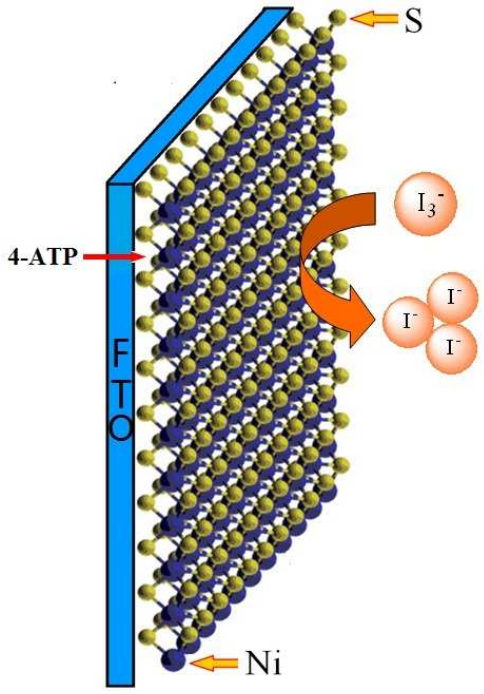

Fig. 1 Schematic of the catalytic mechanisms of NiS* CE.

Fig. 1 gives the possible catalytic mechanisms of NiS* CE for I_3^- reduction during the power conversion process of the DSSC. Since the 4-ATP can be used as an effective bridge across FTO substrate and NiS nanoparticles by -SH group on 4-ATP. Therefore, for the NiS* CE, modification of FTO glass by 4-ATP, the surface roughness and nanoparticles arrangement of NiS thin film are greatly improved, which favors to enhance the adhesion and the contact of the NiS nanoparticles

on the FTO substrates. The CE with desired smooth surface and microporous structure provides good mechanical contact performance. This supplies a large number of charge transport paths, along which the charges can be transferred to the surface of the 4-ATP/NiS easily. Therefore, the NiS* CE is logically to provide a better catalytic activity and R_{ct} toward the reduction of I_3^-.

3.2 Morphology and composition of samples

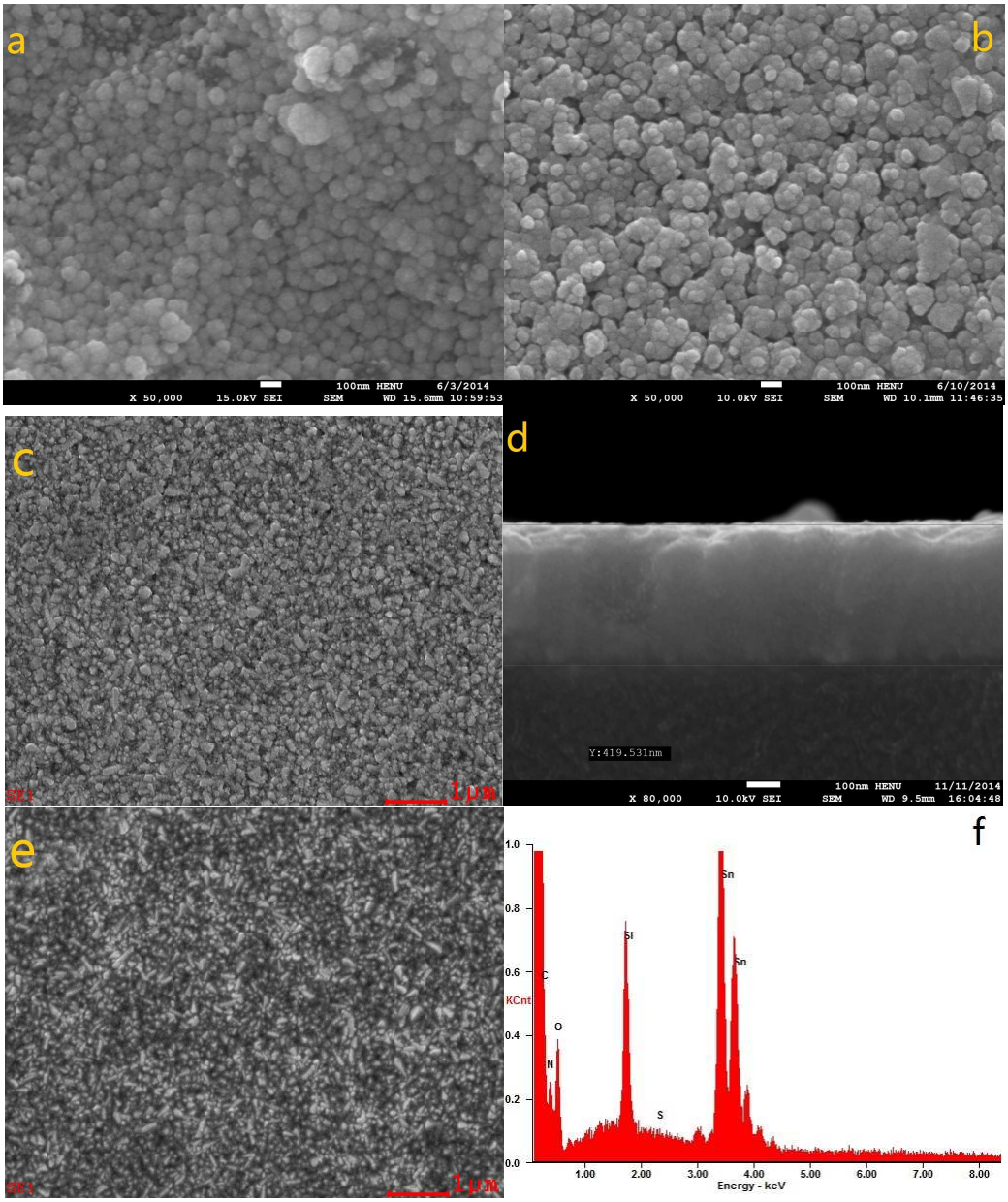

Fig. 2 The SEM images of NiS (a) and NiS* (b) CEs, FTO substrate (c), the cross-sectional of FTO/4-ATP (d) and FTO/4-ATP (e); the EDS image of FTO/4-ATP (f).

According to the previous reports,[22,23] –SH can be well assembled on the FTO surface. To diminish the interfacial resistance and accelerate the charge transport between NiS and FTO glass substrate, 4-ATP was used to form 4-ATP/NiS film. Fig. 2 shows the typical top-view FESEM images of NiS and NiS* films. Fig. 2a exhibits that the NiS particles disorderly coat on the FTO substrate and shows a concavo convex aggregation. Compared to Fig. 2a, the surface morphology of NiS* CE is further improved decorated with 4-ATP, and it presents flat and non-dense surface with a microporous structure as shown as in Fig. 2b. Thus, the microporous structure fortifies the contact with FTO, favors the permeation of I^-/I_3^- electrolyte, and thus accelerates charge transportation, which plays a key role on the performance of the DSSC.[24]

Figs. 2c and 2e show the typical top-view FESEM images of FTO and 4-ATP/FTO films. Compared with FTO film, the 4-ATP/FTO film reveals an improved combination for the FTO via –SH end and guides the growth of NiS to form 4-ATP/NiS film. Furthermore, the thickness of 4-ATP can be estimated of about 69.53 nm from the cross-section view of 4-ATP/FTO film shown in Fig. 2d, which can be validated by the EDS displayed in Fig. 2f.

3.3 Electrochemical properties of NiS CE*

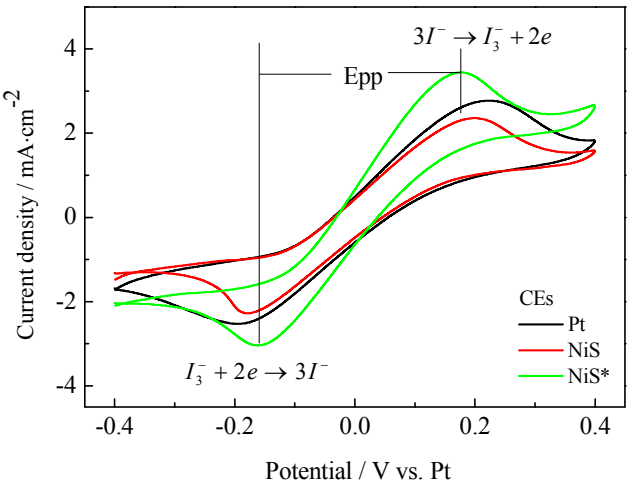

Fig. 3 Cyclic voltammograms for the Pt, NiS and NiS* CEs with the scan rate of 50 mV·s^{-1}.

Fig. 3 shows the CV curves of the Pt, NiS and NiS* counter electrodes with the scan rate of 50 mV·s^{-1} to investigate the electrocatalytic activity of the samples in the potential interval of −0.4 to 0.4 V vs. Pt according to the previous reports.[25,26] Generally, in CV curves, the cathodic peak

current density (I_{pc}) corresponds to the reaction rate of the catalyst for the reduction of I_3^- ions to I^- ions, and a higher I_{pc} absolute value implies better electrocatalytic ability for the catalytic material; the peak-to-peak separation (E_{pp}) and the absolute value of overpotential (V_{pc}) is inversely correlated with the standard electrochemical rate constant of a redox reaction and electrocatalytic ability of the samples.[27] In Fig. 3, the NiS* CE shows a higher I_{pc} absolute value of 3.038±0.01 mA·cm^{-2} than that of Pt (2.543±0.01 mA·cm^{-2}) and NiS (2.245±0.01 mA·cm^{-2}) CEs, demonstrating a much faster rate in I^-/I_3^- electrolyte and high conductivity for the higher cathodic current density of the NiS* CE than that of the others. Also, the NiS* CE is provided with the smallest absolute value of E_{pp} and V_{pc} among the Pt, NiS and NiS* CEs (the detail data listed in Table 1), which indicates that the NiS* CE possesses an excellent electrocatalytic ability for triiodide reduction reaction. It is notable that the NiS CE has low I_{pc} and similar V_{pc} for the reduction of I_3^- to Pt electrode does from the reduction peak position in Fig. 3. However, owing to the bridge effect by 4-ATP, NiS* CE has the larger I_{pc}, which compensates its disadvantage in overpotential and gets an improved V_{pc}. Therefore, the NiS* CE is adopted as an efficient CE in DSSC.

Simultaneously, the diffusion coefficient (D_n) is proportional to the I_{pc}, which obeys the Randles-Sevcik equation as following.[28]

$$I_{pc} = Kn^{1.5}AC(Dn)^{0.5}v^{0.5}$$

where I_{pc} is the cathodic current densities; K is the constant of 2.69×10^5; n means the number of electrode contributing to the charge transfer (here n=2); A is the area of the CE; C and v represent the concentration of I_3^- species and the scan rate, respectively. Thus, from which, the diffusion coefficients of I_3^- for the Pt, NiS and NiS* CEs are estimated to be 3.10×10^{-6}, 2.42×10^{-6} and 4.43×10^{-6} cm^{-2}·s^{-1}, respectively. The diffusivity for the NiS* CE is slightly larger than that of the Pt and NiS CEs, presumably due to the improvement in the surface roughness of the CE.

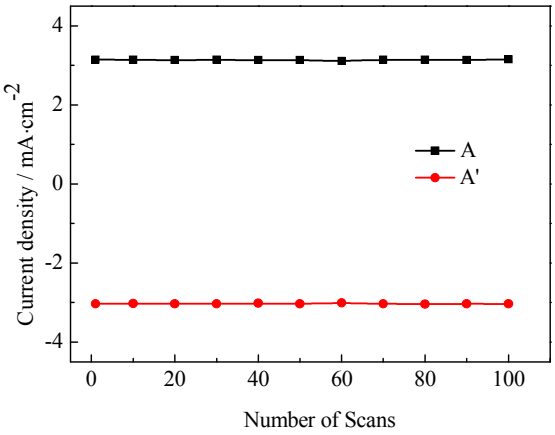

Fig. 4 The relationship between the number of CV scans and the maximum redox peak currents in the I^-/I_3^- system for NiS* CE at a scan rate of 50 $mV \cdot s^{-1}$.

Fig. 4 shows the relationship between the 100 successive CV cycles and the maximum redox peak currents in the I^-/I_3^- system for NiS* CE at a scan rate of 50 $mV \cdot s^{-1}$. Both redox peak current densities keep at the same locations with the cycle number increasing. It can be concluded that the NiS* CE possesses good chemical stability and is tightly coated on the FTO substrate.[29]

Table 1 The electrochemical performance parameters obtained from EIS and CV based on the various counter electrodes.

CEs	R_s ($\Omega \cdot cm^2$)	R_{ct} ($\Omega \cdot cm^2$)	Z_w ($\Omega \cdot cm^2$)	I_{pc} ($mA \cdot cm^{-2}$)	$\lvert E_{pp} \rvert$ (V)	$\lvert V_{pc} \rvert$ (V)	J_0 ($mA \cdot cm^{-2}$)	J_{lim} ($mA \cdot cm^{-2}$)
Pt	6.26±0.01	3.55±0.01	1.47±0.01	-2.543±0.01	0.412±0.01	0.189±0.01	0.46±0.01	1.83±0.01
NiS	6.17±0.01	4.11±0.01	3.96±0.01	-2.245±0.01	0.383±0.01	0.176±0.01	0.17±0.01	1.51±0.01
NiS*	6.31±0.01	3.07±0.01	0.39±0.01	-3.038±0.01	0.329±0.01	0.159±0.01	0.76±0.01	2.08±0.01

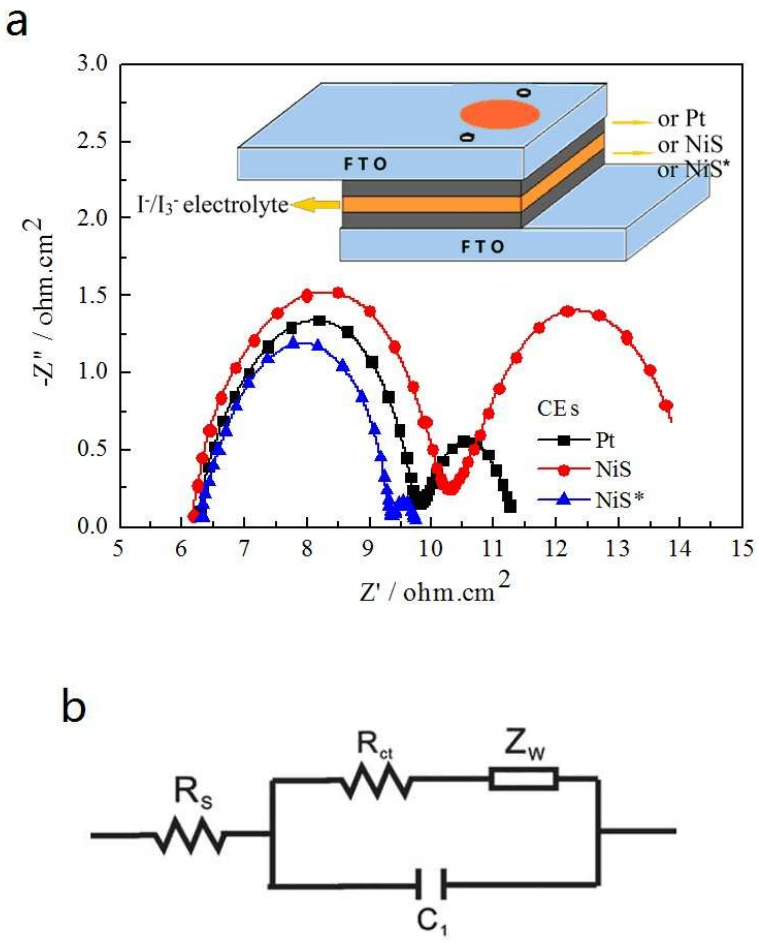

Fig. 5 Nyquist plots of the symmetrical Pt, NiS and NiS* CEs for I^-/I_3^- redox couple (a) and the relevant equivalent circuit model (b).

The interfacial electrochemical behaviors between CE and electrolyte are further evaluated by EIS using a symmetric dummy cell configuration consisting of two identical CEs (CE/electrolyte/CE). Fig. 5 shows the Nysquist plots of the symmetric cells of the Pt, NiS and NiS* CEs with the first semicircle in the middle frequency range which represents the resistance against the heterogeneous electron transfer at the electrode/electrolyte interface (R_{ct}), and the values of R_{ct} were listed in Table 1. Fig. 5b shows the relevant equivalent circuit model, in which R_s estimated from the intercept on the real axis in the high-frequency region is the series resistance of CEs. The semicircle at low frequency corresponds to the Nernst diffusion impedance (Z_w) of the I^-/I_3^- redox couple in electrolyte.[30] From Fig. 5a, the R_s for NiS and NiS* CEs are 6.17±0.01 and 6.31±0.01 $\Omega \cdot cm^{-2}$, respectively, which have a similar value to the Pt CE (6.26±0.01$\Omega \cdot cm^{-2}$),

indicating the electrocatalytic materials are firmly bonded to the FTO substrates. The R_{ct} among the Pt, NiS and NiS* CEs, decreased in the order of NiS (4.11±0.01 $\Omega \cdot cm^{-2}$) > Pt (3.55±0.01 $\Omega \cdot cm^{-2}$) > NiS* (3.07±0.01 $\Omega \cdot cm^{-2}$). It is clearly that the R_{ct} of NiS* CE is much lower than that of Pt and NiS electrodes, confirming the comparable catalytic abilities of the NiS* CE in I^-/I_3^- electrolyte. Furthermore, the Z_w of NiS* CE is found of 0.39±0.01 $\Omega \cdot cm^2$, which is smaller than that of Pt (1.47±0.01 $\Omega \cdot cm^2$) and NiS (3.96±0.01 $\Omega \cdot cm^2$) counter electrodes. These results are well consistent with the CV test. This can be attributed to an effective bridge across FTO substrate and NiS nanoparticles by -SH group on 4-ATP. Therefore, the enhanced electrocatalytic activity for the NiS* CE can make electrons transmit across the CE|FTO interface easily, which is beneficial to improve the photovoltaic performance of the DSSCs (see Table 2).[31]

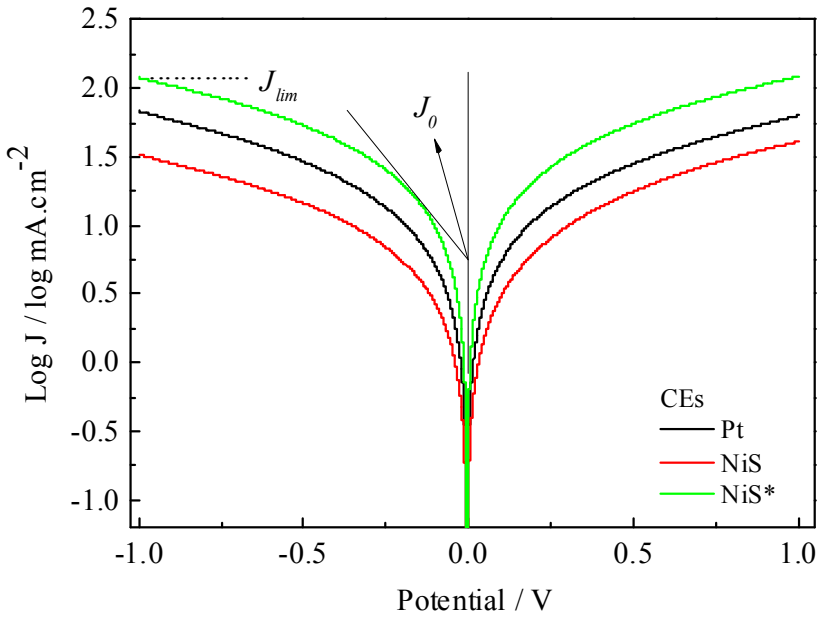

Fig. 6 Tafel curves of the symmetrical Pt, NiS and NiS* counter electrodes.

Tafel-polarization measurements are carried out in a dummy cell similar to the ones used in EIS to aid investigation the interfacial charge-transfer properties of the I^-/I_3^- redox couple on the CEs. Fig. 6 shows the Tafel curves of the Pt, NiS and NiS* CEs in I^-/I_3^- redox couple. The curves present logarithmic current density as a function of potential and thus the corresponding exchange current density (J_0) for each CE can be evaluated, as also listed in Table 1. The exchange current density (J_0) is tantamount to the catalytic activity of the electrode; the limiting diffusion current

density (J_{lim}) is positively relevant to the diffusion coefficient, which corresponds to the diffusion behavior of the I^-/I_3^- redox couple in the electrolyte. Therefore, according to the slopes for the anodic or cathodic branches, J_0 follows the order of NiS* > Pt > NiS, implying an excellent electrocatalytic ability for the I^-/I_3^- electrolyte. The relationship between J_0 and R_{ct} of counter electrode for the reduction of I_3^- ions to I^- ions is also can be calculated by Eqn. (3). Moreover, as shown as Fig. 6 and Table 1, J_{lim} follows the same order as J_0, revealing a higher diffusion velocity for the NiS* CE in I^-/I_3^- electrolyte after modification of FTO glass by 4-ATP. In summary, according to the systematic evaluation of electrocatalytic activity for the NiS* CE, it is as effective and sufficient as Pt to catalyze the reduction reaction of triiodide to iodide.

3.4 Photovoltaic performance of DSSCs with NiS electrode*

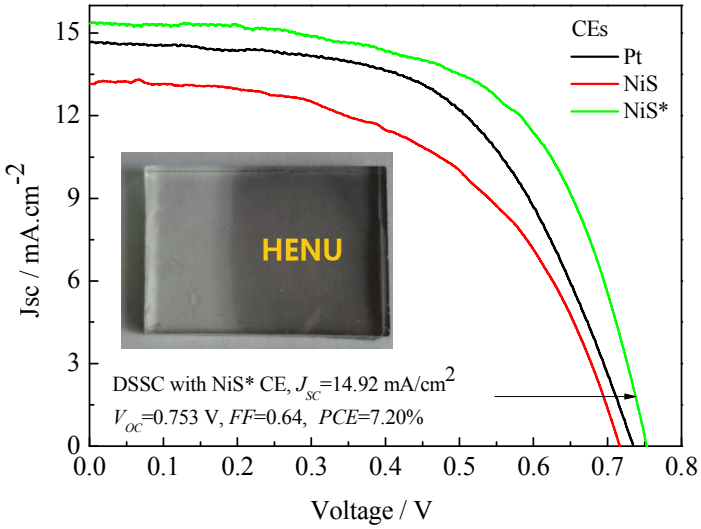

Fig. 7 *J-V* characteristics of the DSSCs fabricated with different CEs under the standard illumination.

Fig. 7 presents the photovoltaic performance of the DSSCs based on Pt, NiS and NiS* CEs under the irradiation of 100 mW·cm^{-2}, and the photovoltaic parameters are given in Table 2. From the *J-V* curves and Table 2, it is found that the DSSCs with the Pt and NiS CEs exhibit the power conversion efficiencies (*PCEs*) of 6.27% and 5.16%, respectively (details of photovoltaic parameters as seen in Table 2). The DSSC with NiS* CE presents J_{sc} of 14.92 mA·cm^{-2}, V_{oc} of 0.753V, *FF* of 0.64, and resulting in a good *PCE* of 7.20% comparing with that for the ones using the Pt and NiS CEs. The enhancement in photovoltaic performance for the DSSC NiS*-based

should be mainly originating from the excellence of the counter electrode, such as microporous morphology, good electrochemical catalytic ability, low charge transfer resistance and contact between electrolyte/CE interface as indicated in the aforementioned FESEM, CV, EIS and Tafel polarization plots.

Table 2 The photovoltaic performance parameters of DSSCs with various counter electrodes.

Cells	V_{oc} (V)	J_{sc} (mA·cm^{-2})	*FF*	*PCEs* (%)
Pt-based	0.734	14.23	0.60	6.27
NiS-based	0.716	12.88	0.56	5.16
NiS*-based	0.753	14.92	0.64	7.20

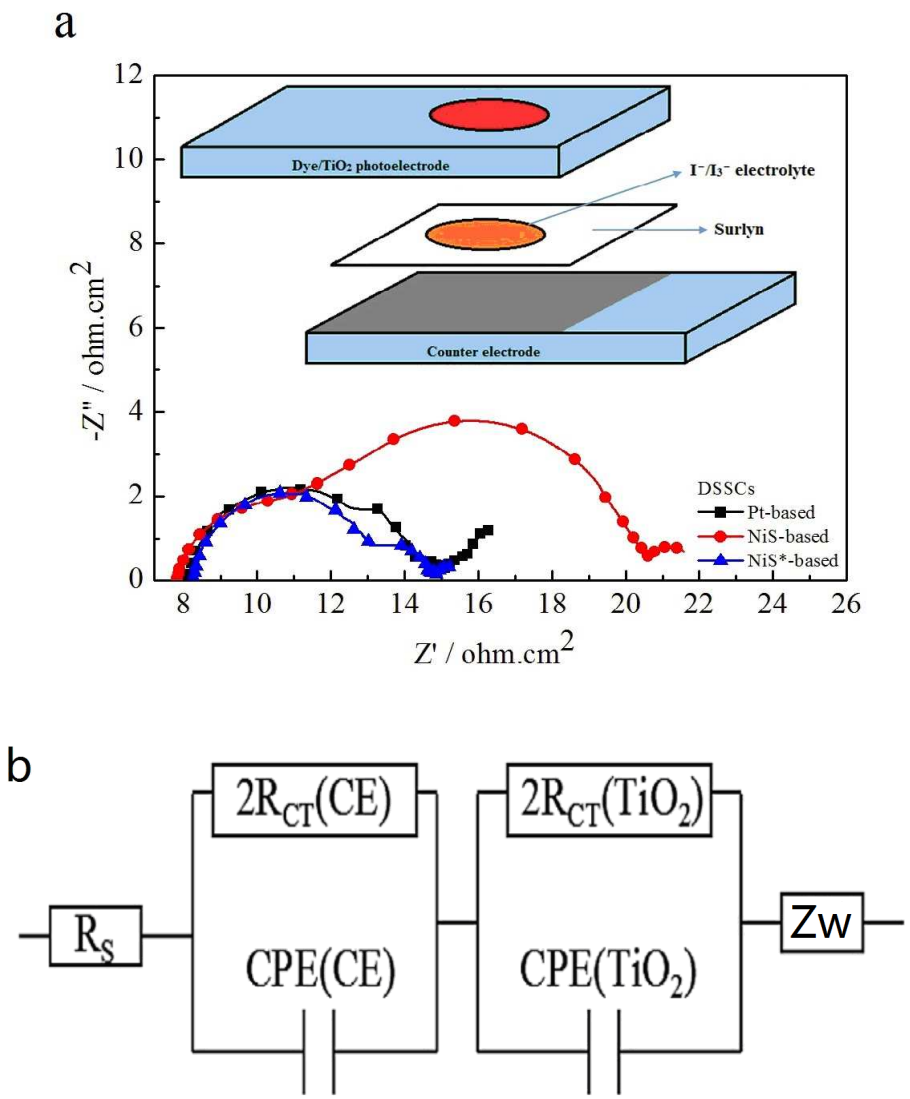

Fig. 8 EIS spectra of DSSCs with the Pt, NiS and NiS* CEs (a) and the relevant equivalent circuit model (b).

Fig. 8a shows the Nyqyist plots of the DSSCs based on the Pt, NiS and NiS* CEs with the frequency range of 10^{-1}-10^{5} Hz and the schematic of solar cell displays in the inset. The relevant equivalent circuit model is as shown as Fig. 8b. The first semicircle at high frequency represents the R_{CT} (CE), which is the electron transfer resistances at the CE|electrolyte interface and the working electrode (WE)|electrolyte interface and is vital for its operation. While the second semicircle at middle frequency is the R_{CT} (TiO_2) for the charge-transfer resistance at the electrolyte/anode interface, and the third semicircle at low frequency stands for the Nernst diffusion impedance (Z_w) on the diffusion resistance of the I^-/I_3^- redox species and is unimportant for the performance of DSSC.[32] From Fig. 8, the DSSC based on the NiS* CEs displays the smallest R_{CT} (CE) among the ones with the Pt, NiS and NiS* CEs, indicating the fastest electron transport and highest performance occurred in the DSSC.[33] The lower R_{CT} (CE) signifies the higher *FF* and the higher *PCE*.[33] Therefore, it can be concluded from Fig. 8 that the excellent electrocatalytic ability of the NiS* CE facilitates fast electron transport at the interface between electrolyte and the electrodes for the I^-/I_3^- redox reaction and higher J_{sc} and V_{oc} obtained.

4. Conclusions

A novel NiS* film was prepared by two-step chemical/electrochemical process coated on FTO substrate. 4-ATP modified FTO surface and was used as a bridging agent via a covalent bonding between FTO and -SH end on 4-ATP and an in-situ growth of NiS chain end on 4-ATP to accelerate the charge transfer from FTO to NiS. A much better electrochemical behavior to iodide/triiodide for the NiS* CE was verified from electrochemical tests (CV, EIS and tafel), and guaranteed the fast mass transport at the interface of electrolyte-electrode. The DSSC assembled with NiS* CE acquits efficient photoelectric behaviors with respectable values of J_{sc}, V_{oc} and *FF*. Consequently, a much higher power conversion efficiency of 7.20% has been achieved as comparing to that of the DSSC based on Pt electrode (6.27%). The results carry a foreshadowing for the development of a new generation of high performance, low-cost DSSCs using composite CEs.

Acknowledgements

The authors are very grateful to the joint support by the National Natural Science Foundation of China (No.61306019) and the National Natural Science Foundation of China (No. 21103041). This work is also supported by the Natural Science Foundation of Henan Educational Committee (No. 14A430023), the Scientific Research Found of Henan Provincial Department of Science and Technology (No. 132300413210) and the Natural Science Foundation of Henan University (No. 2013YBZRO47).

References

1 B. O'Regan and M. Grätzel, *Nature*, 1991, **353**, 737–740.

2 A. Yella, H. W. Lee, H. N. Tsao, C. Yi, A. K. Chandiran, M. K. Nazeeruddin, E. W. Diau, C. Y. Yeh, S. M. Zakeeruddin and M. Grätzel, *Science*, 2011, **334**, 629–634.

3 A. Hagfeldt, G. Boschloo, L. Sun, L. Kloo and H. Pettersson, *Chem. Rev.*, 2010, 110, 6595-6663.

4 C. Yoon, R. Lee, W. Chae and K. Kim, *Electrochim. Acta*, 2008, **53**, 2890–2896.

5 G. Khelashvili, S. Behrens, C. Weidenthaler, C. Vetter, A. Hinsch, R. Kern, K. Skupien, E. Dinjus and H. Bonnemann, *Thin Solid Films*, 2006, **511**, 342–348.

6 V. Dao, S. Kim, H. Choi, J. Kim, H. Park and J. Lee, *J. Phys. Chem. C*, 2011, **115**, 25529-25534.

7 A. Kay and M. Grätzel, *Sol. Energy Mater. Sol. Cells*, 1996, 44, 99–117.

8 F. Hao, Z. Wang, Q. Luo, J. Lou, J. Li, J. Wang, S. Fan, K. Jiang and H. Lin, *J. Mater. Chem*., 2012, **22**, 22756–22762.

9 T. Chen, L. Qiu, Z. Yang, Z. Cai, J. Ren, H. Li, H. Lin, X. Sun and H. Peng, *Angew. Chem., Int. Ed*., 2012, **51**, 11977–11980.

10 L. Kavan, J. Yum and M. Grätzel, *Nano Lett.*, 2011, 11, 5501–5506.

11 G. T. Yue, J. H. Wu, Y. M. Xiao, J. M. Lin, M. L. Huang and Z. Lan, *J. Phys. Chem. C*, 2012, **116**, 18057–18063.

12 Q. H. Li, J. H. Wu, Q. W. Tang, Z. Lan, P. J. Li and J. M. Lin, *Electrochem. Commun.*, 2008, **10**, 1299–1302.

13 L. J. Sun, Y. Bai and K. N. Sun, *RSC Adv.*, 2014, **4**, 42087–42091.

14 G. T. Yue, J. H. Wu, Y. M. Xiao, M. L. Huang, J. M. Lin and J. Y. Lin, *J. Mater. Chem. A*, 2013, **1**, 1495–1501.

15 Z. L. Hu, K. Xia, J. Zhang, Z. Y. Hu and Y. J. Zhu, *RSC Adv.*, 2014, **4**, 42917–42923.

16 G. Li, J. Song, G. Pan and X. Gao, *Energy Environ. Sci.*, 2011, **4**, 1680–1683.

17 M. Wu, J. Bai, Y. Wang, A. Wang, X. Lin, L. Wang, Y. Shen, Z. Wang, A. Hagfeldt and T. Ma, *J. Mater. Chem.*, 2012, **22**, 11121–11127.

18 H. C. Sun, D. Qin, S. Q. Huang, X. Z. Guo, D. M. Li, Y. H. Luo and Q. B. Meng, *Energy Environ. Sci*., 2011, **4**, 2630–2637.

19 Z. L. Ku, X. Li, G. H. Liu, H. Wang, Y. G. Rong, M. Xu, L. F. Liu, M. Hu, Y. Yang and H. W. Han, *J. Mater. Chem. A*, 2013, **1**, 237–240.

20 G. T. Yue, J. H. Wu, J.-Y. Lin, Y. M. Xiao, J. M. Lin, M. L. Huang and Z. Lan, *Carbon*, 2013, **55**, 1–9.

21 G. T. Yue, X. P. Ma, Q. W. Jiang, F. R. Tan, J. H. Wu, C. Chen, F. M. Li and Q. H. Li, *Electrochim. Acta*, 2014, **142**, 68–75

22 A. C. T. Alves, D. J. C. Gomes, J. R. Silva and G. B. Silva, *Appl. Surf. Sci*., 2013, **279**, 67–70.

23 P. T. Bui, T. Nishino, Y. Yamamoto and H. Shiigi, *J. Am. Chem. Soc.*, 2013, **135**, 5238–5241.

24 M.-Y. Yen, C.-K. Hsieh, C.-C. Teng, M.-C. Hsiao, P.-I. Liu, C.-C.M. Ma, M.-C. Tsai, C.-H. Tsai, C.-H. Tsai, Y.-R. Lin and T.-Y. Chou, *RSC Adv*., 2012, **2**, 2725–2728.

25 G. T. Yue, W. F. Zhang, J. H. Wu and Q. W. Jiang, *Electrochim. Acta*, 2013, **112**, 655–662.

26 J. Y. Lin, J. H. Liao and T. Y. Hung, *Electrochem. Commun*., 2011, **13**, 977–980.

27 K. Saranya, N. Sivasankar and A. Subramania, *RSC Adv*., 2014, **4**, 36226–36233.

28 A. Hauch, A. Georg, *Electrochim. Acta*, 2001, **46**, 3457–3466.

29 G. T. Yue, X. A. Zhang, L. Wang, F. R. Tan, J. H. Wu, Q. W. Jiang, J. M. Lin, M. L. Huang and Z. Lan, *Electrochim. Acta*, 2014, **129**, 229–236.

30 P. Zhai, Y.-H. Chang, Y.-T. Huang, T.-C. Wei, H. J. Su and S.-P. Feng, *Electrochim. Acta*, 2014, **132**, 186–192.

31 J. Chen, B. Li, J. Zheng, J. Zhao, H. Jing and Z. Zhu, *Electrochim. Acta*, 2011, **56**, 4624−4630.

32 Y. Zheng, X. Tao, L. Wang, H. Xu, Q. Hou and W. Zhou, *Chem. Mater*., 2010, **22**, 928−934.

33 L. Heng, X. Wang, N. Yang, J. Zhai, M. Wan and L. Jiang, *Adv. Funct. Mater*., 2010, **20**,

266–271.